Performance of the SLD Central Drift Chamber*

M.D. Hildreth, T.R. Junk, T.W. Markiewicz, H. Masuda, B. Mours[a], H.A. Neal, C.Y. Prescott,
L.S. Rochester, A. Sugiyama[b], T. Takahashi[c], T. Usher, C.C. Young
Stanford Linear Accelerator Center, Stanford University, Stanford, CA 94309

R. Shypit
University of British Columbia, Vancouver, BC V6T 1Z1, Canada

M.J. Fero, D.C. Williams[d]
Massachusetts Institute of Technology, Cambridge, MA 02139

R. Massetti
INFN Sezione di Perugia and Università di Perugia, I-06100 Perugia, Italy

J. Venuti
Vanderbilt University, Nashville, TN 37235

A. Honma
University of Victoria, Victoria, BC V8W 3P6, Canada

Abstract

We report for the first time on the performance of the SLD Central Drift Chamber (CDC) at SLC, which has been recording data since 1992. The low mass of the chamber and the use of a gas characterized by both a low drift velocity and low diffusion constant help to minimize the drift-distance measurement errors. We describe some of the calibrations and corrections applied to the data, and report on the resolutions achieved thus far.

We measure an intrinsic drift resolution of 55-110 μm in the region of uniform field. Analysis of the full drift-pulse waveform allows for efficient double-hit resolution of about 1 mm. Momentum resolution is characterized by the formula $(dp_t/p_t^2)^2 = 0.0050^2 + (0.010/p_t)^2$. Used in conjunction with the SLD vertex detector, the CDC permits measurements of impact parameters of high-momentum tracks to the level of 10 μm in the r-φ plane and 36 μm in the r-z plane. A resolution of 6.4% is achieved in the measurement of dE/dx for the electrons in Bhabha scattering events.

I. INTRODUCTION

The Central Drift Chamber (CDC) of the SLAC Large Detector (SLD) tracks charged particles over 80% of the solid angle of SLD, and operates in a uniform solenoidal magnetic field of 0.6 Tesla. It has been taking data at the Stanford Linear Collider (SLC) since 1992, and has recorded over 100,000 Z^0 decays in that period. Analysis of the accumulated data sample has allowed us to study the performance of the CDC, and to perform the calibrations necessary to begin to realize the potential of the chamber.

After describing the construction of the CDC, its high voltage system, gas composition, and electronics, we will outline our track reconstruction algorithm, and highlight some aspects of the chamber performance.

II. CHAMBER DESCRIPTION

A. Construction Parameters

The CDC is a cylindrical annulus with a length of 2 m, an inner radius of 20 cm and an outer radius of 1 m. It was constructed by stringing wires through a pre-assembled rigid low-mass shell consisting of dished aluminum end plates, 5 mm thick, and inner and outer cylinders made of a laminate of aluminum sheet and Hexcel fiberboard. As shown in fig. 1, the chamber contains 80 layers of sense wires arranged in 10 superlayers of 8 wires each. Wire length varies from 169 cm to 179 cm. Six superlayers have a 41-mrad stereo angle with respect to the beam axis. Each superlayer is made of independent cells roughly 6 cm wide by 5 cm high. The sense wires and the field wires separating adjacent cells are aligned on radii of the chamber. Figure 2 shows a detail of one such cell.

The field-shaping wires as well as those providing the high field for charge amplification are made of 150-μm gold-coated aluminum wire, while the sense wires are 25-μm gold-coated tungsten. Aluminum (tungsten) wires are crimped into aluminum (stainless steel) pins, which are themselves crimped into larger diameter bushings. The field-shaping wire pins are

---

Contributed to the IEEE Transactions of Nuclear Science, Proceedings of the IEEE Nuclear Science Symposium, Norfolk, VA, October 30 - November 5, 1994

supported by Celanex feedthroughs cold pressed into the chamber endplate. The central guard-sense wire assemblies were strung separately off the chamber, with the pin ends supported by Lexan blocks, and then installed as units in the CDC and brought back to their nominal wire tensions through a set of adjustment screws. Wire tensions were measured by exciting transverse oscillations of the wire in an external transverse magnetic field and measuring the frequency of the induced signal after the driving pulse died away. Aluminum guard (field) wires were strung in 1988-1989 at 500 (400) gm tension to allow for tension reduction after wire "creep". The sense wires were strung at 100 gm tension.

B. High Voltage

The high voltage system is composed of 20 independent power supplies for each layer. The guard wire voltage is set to 3027 V for each layer to equalize the chamber gain. The field wire voltages are chosen to make the functional dependence of electric field on drift distance uniform over the 80 wire layers of the chamber. The mean drift field is 0.9 kV/cm; the mean field wire voltage is about 5300 V. Fields at the wire surfaces are highest for the field wires at the cell corners, where they rise to over 40 kV/cm. Concerns about wire aging, and about electrostatic instability, limit the voltage on the chamber.
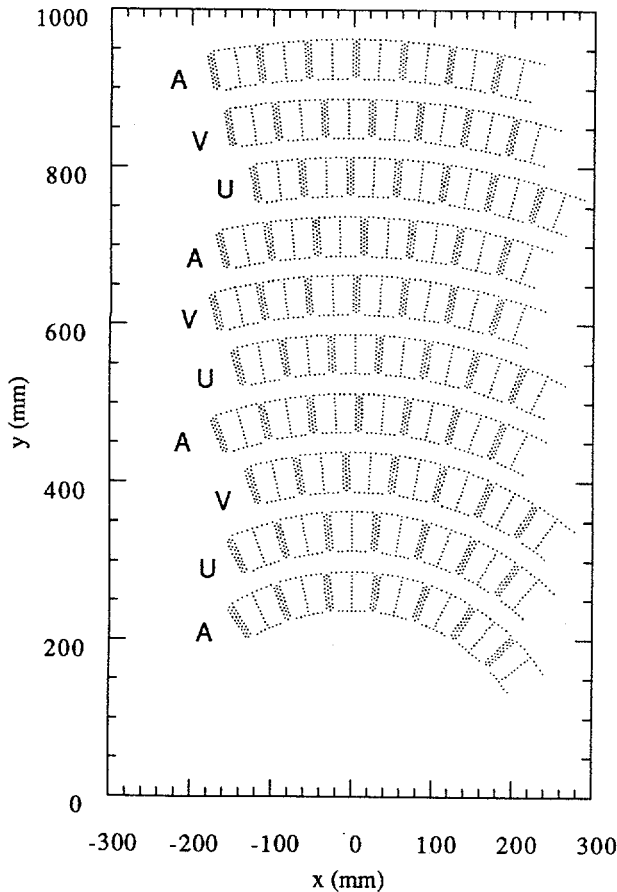
Because the endplates are grounded, the electric field is reduced there, and the chamber volume within approximately 5 cm of the endplate is inefficient.

C. Gas

CO_2 was chosen as the primary component of the gas mixture because of its low drift velocity and low diffusion constant. The former property allows for a finer sampling of the pulse for a fixed electronics speed; the latter reduces the contribution of diffusion to the resolution. Isobutane was added as a quencher at a level low enough to keep the mix nonflammable and to thus minimize safety problems. Because the chamber voltage was limited by considerations already mentioned, argon was added to increase the gain to the desired level. Water was added after gas aging tests[1] indicated its presence could ameliorate the effects of wire aging in the then unknown radiation environment of SLC. The final gas mixture is 75% CO_2, 21% Argon, 4% Isobutane, and 0.2% water and has a drift velocity of 7.9 μm/ns at the mean drift field.

The chamber is protected from contamination by atmospheric oxygen by flowing the mixed gas at a rate of one exchange each 10 hours and by flowing pure CO_2 in the electronics volume formed by the endplates and the sealed, copper-plated aluminum covers. At the resulting 60 ppm level of oxygen, electrons are not appreciably absorbed as they drift over the full distance of a cell.

Fig. 1. Partial view of the CDC endplate showing the 10 layers. Axial layers are labeled 'A', while the stereo layers are labeled 'U' and 'V'.
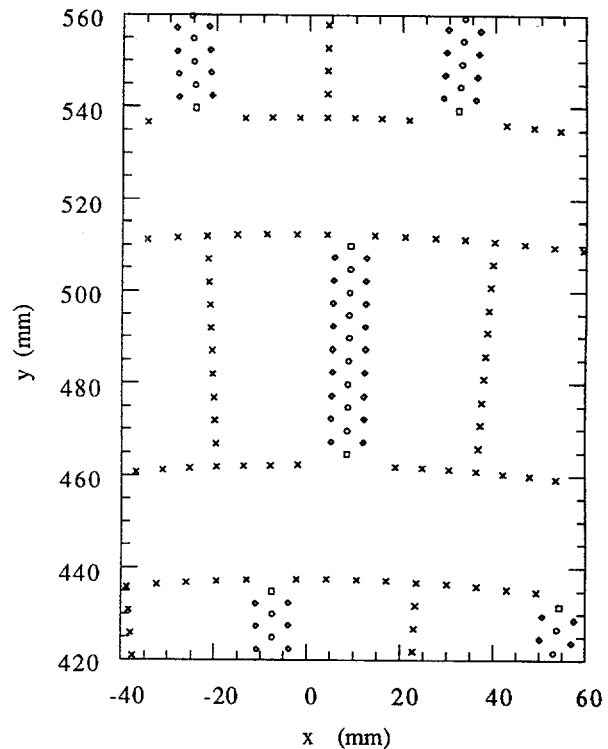

Fig. 2. Wire layout of a single cell in an axial layer of the SLD drift chamber. The 8 sense wires (circles) are surrounded by a grid of guard wires (diamonds and squares). The field-shaping wires are shown as x's.

2

DISCLAIMER

Portions of this document may be illegible in electronic image products. Images are produced from the best available original document.

One disadvantage of our gas mix is that the drift velocity depends significantly on the gas density and composition, and on the electric field. The CDC is maintained at a constant temperature of 20° C by a series of cooling tubes attached to each endplate and to an external precision heat exchanger system. However, no attempt is made to stabilize it against fluctuations in atmospheric pressure.

D. Readout Electronics

The CDC readout electronics[2] were designed to operate in the 120-Hz pulsed beam of the SLC. At each beam crossing, the waveform of the charge deposited on each sense wire is sampled and stored at 119 MHz onto a hybridized 512-channel switched capacitor array called an Analog Memory Unit[3] (AMU). For triggered events the stored waveform from each end of 64 wires is digitized by two 12-bit fast ADCs and the data transported serially over optical fibers into a FASTBUS Waveform Sampling Module (WSM). This double-ended readout, combined with the 330-Ω resistance of the sense wires, permits a charge division measurement of the axial (z)
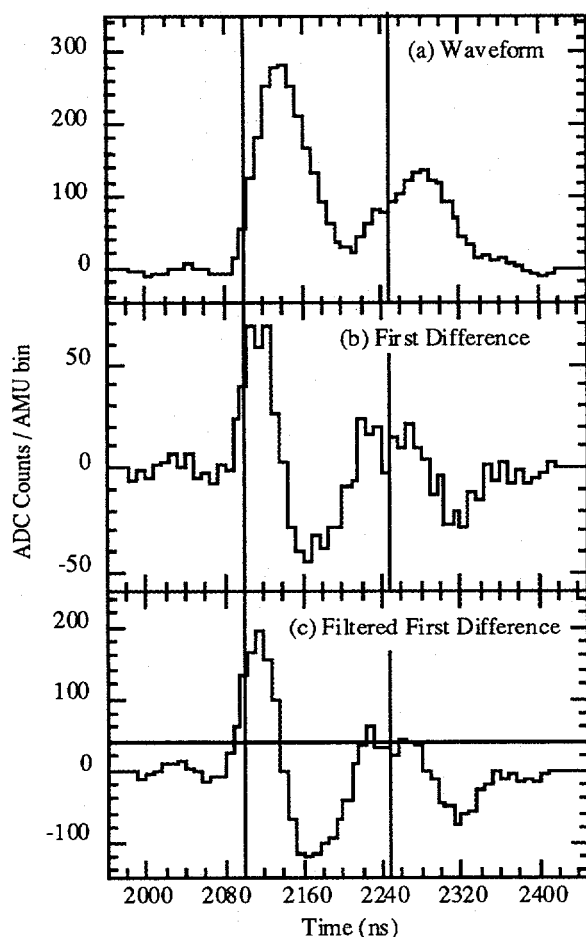

Fig. 3. A typical waveform with two resolved hits. Part (a) shows the waveform itself, part (b) shows the difference of adjacent bins, part (c) shows the difference with the filter described in the text. The vertical lines indicate the times assigned to each hit. The horizontal line in (c) is the threshold for detecting a hit.
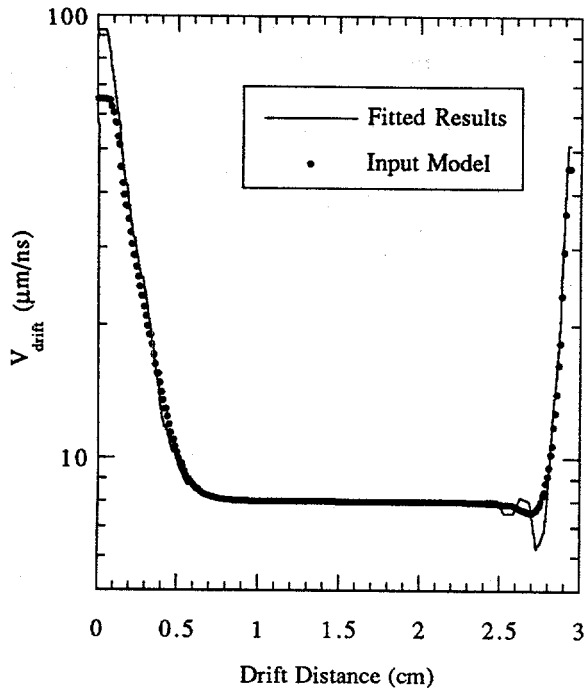
coordinate accurate to about 5 cm, to aid in later track finding. The WSM incorporates a Digital Correction Unit[4] (DCU), a Motorola 68020 processor, and digital memory. The DCU applies an eight-segment piece-wise-linear calibration to each AMU channel and provides for zero-suppression. In order to further reduce the volume of data written to tape, the processor analyzes the waveforms to find chamber hits, and extracts the time, charge, pulse height, and pulse width of each hit at each end of the wire, as described below.

III. DATA REDUCTION

A. Waveform Analysis

Figure 3 shows a multi-hit waveform. The waveform analysis proceeds in two steps. First, the beginning and end of a single pulse are identified by examining a filtered first difference of the waveform (fig. 3c). The beginning of a pulse is where this distribution rises above a threshold set to discriminate against noise; the end, where it returns to the baseline from the negative side.

In the second step, we calculate the time of the leading edge, integrated charge, and pulse height for each pulse. The leading edge time is determined by searching the first difference of the waveform (fig. 3b) for the maximum in the vicinity of the beginning of the pulse, and then computing the weighted average of seven differences about this maximum. The weights are chosen to emphasize the front of the pulse. The charge is the sum of pulse heights above baseline in the waveform (fig. 3a).

The two pulses in the waveform of fig. 3 have quite different risetimes. This variability leads to uncertainty in determining the true time of the pulse, and contributes to tails in the distributions of the hit residuals, as will be discussed below.

B. Track Reconstruction

Track reconstruction proceeds offline, in four stages. First, the time and charge information from both ends of each wire are combined to yield the distance of each hit from its sense wire and its location along the wire.

Next, hits from different wires within a cell are grouped into vector hits (VHs), having a position and direction. This step reduces the number of independent entities presented to the next stage, and eliminates isolated hits. Since our sense wires are not staggered, each set of hits produces two VHs, one on either side of the sense wire plane. At this stage, the hit positions are corrected for the effects of track angle in the bend plane.

The VHs are the input to the next stage, track-finding. The search for tracks starts by finding all combinations of axial VHs which lie on circles, and then adding VHs from stereo layers which fit on these circles. The information from the charge division measurement is used to project the stereo VHs onto the circles. In the first instance, we consider only tracks with ten VHs. Among these, the one with the best χ^2 is

3

Fig. 4. Drift velocity as a function of distance.

Fig. 5. Measured drift velocity correction as a function of time in days. Overall variation in correction is about 1.0% during two summer months.

called a candidate track, and its VHs are removed from further consideration. After identifying all tracks with ten VHs, the algorithm begins again, this time searching for tracks with nine VHs, and continues until all tracks of at least three VHs are found.

Finally, all track candidates are processed by an iterative track fitter, which does a detailed swim, taking into account the variation of the magnetic field, energy loss, and the material in the chamber. The fitter uses the individual hits in the candidate tracks, and may add or delete hits as the iterations proceed. Note that at this stage, z information is provided by the stereo layers. About 1.5% of the track candidates are dropped at this stage, because the χ^2 of the fit is larger than our cutoff value.

IV. DRIFT VELOCITY CALIBRATION

To maximize tracking efficiency, we use hits from all areas of the cell, including those regions near the sense and field-shaping wires, where the electric field is changing rapidly. An electrostatic model and a first estimate of the relationship of drift velocity to electric field are employed to obtain a model of the time-to-distance relationship for each layer. The data are then used to iteratively correct this first estimate by minimizing the fit residuals as a function of drift distance. Figure 4 shows the input and final iteration of the drift velocity as a function of the drift distance in one of the 80 wire layers.

Because the chamber is constructed of alternating axial and stereo layers, and because the electrostatic isolation between adjacent layers is not perfect, the exact field at any z position in a layer depends on the relative position of the adjacent layers. This affects the drift velocity, by as much as 2% for
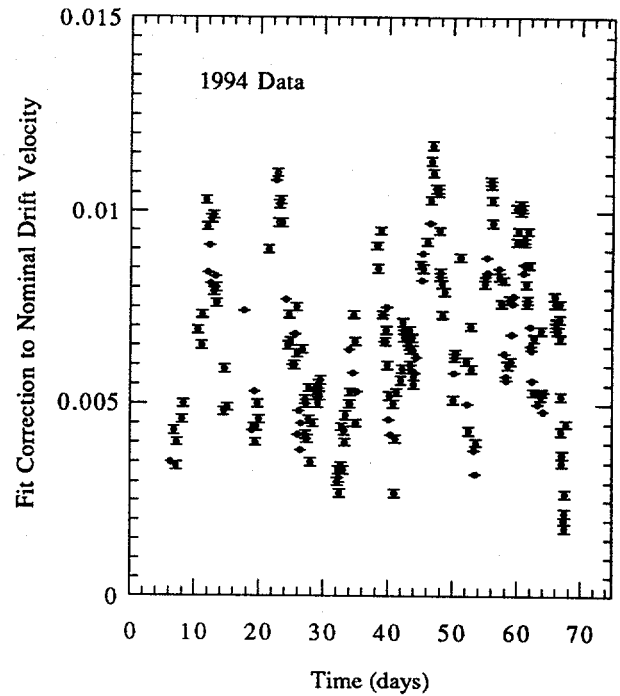
the wires closest to the edge of the layer, and must be compensated for to achieve the best resolution.

As the CDC is maintained at constant temperature, the electron drift velocity (v_d) is expected to vary inversely with
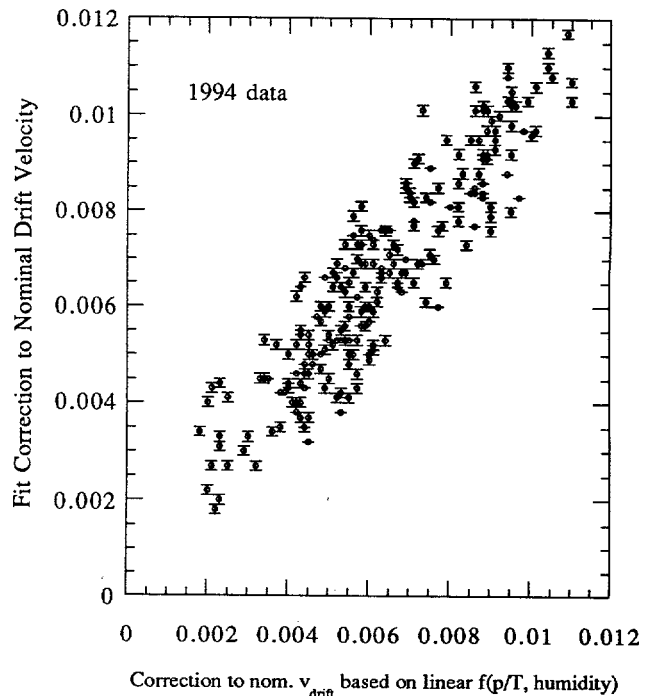

Fig. 6. Measured correction to the nominal drift velocity plotted against the correction calculated based on a linear function of pressure, temperature, and the concentration of water vapor in the gas.
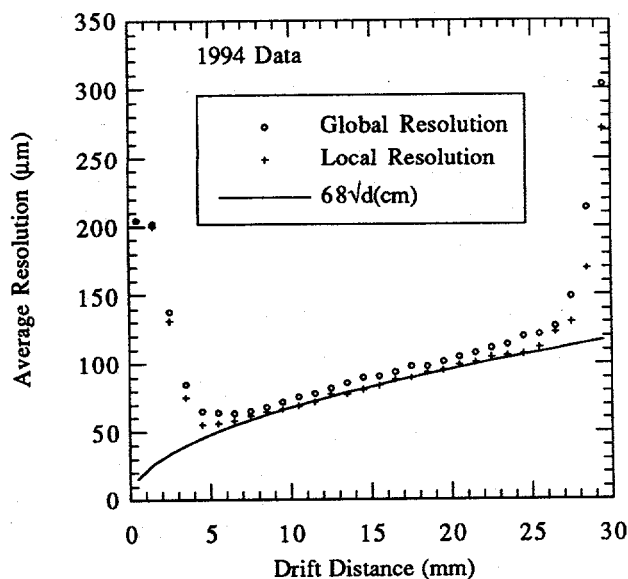
4

Fig. 7. Global and Local resolution as a function of drift distance in a cell.
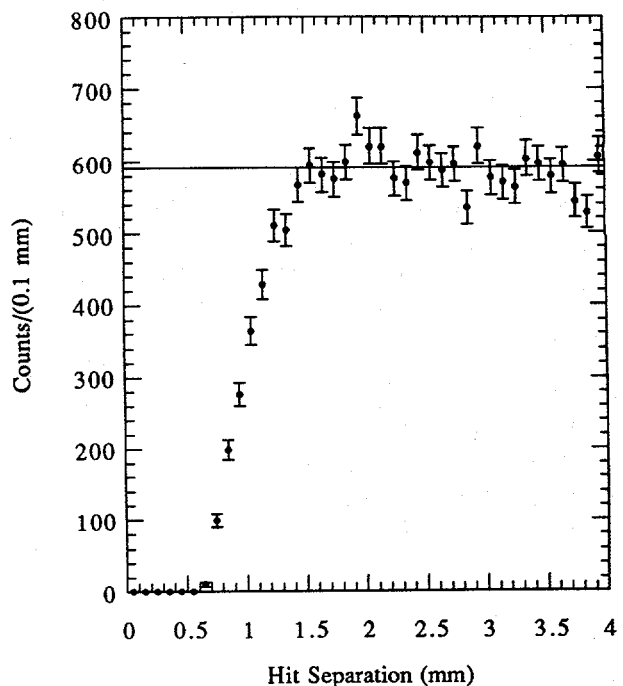

Fig. 8. The number of second hits on a given wire as a function of the separation between the first and second hit, where both hits are on tracks. The horizontal line indicates the level of counts corresponding to full efficiency. 50% efficiency is achieved at a separation of 1 mm.

the pressure about its nominal value of 7.9 μm/ns. The other important parameter which affects the velocity is the concentration of water vapor in the gas. Reconstructed tracks are used to measure changes in v_d by allowing the drift velocity to be one of the variables in the track fit. The value of v_d is determined for each four-hour run by averaging the values obtained for individual tracks. The overall change in the drift velocity can be as much as 2%; fig. 5 shows the fractional correction to the nominal drift velocity vs. time during a two-month running period. These points can be fit to a function of the pressure, temperature and water vapor concentration. Figure 6 shows the measured correction plotted against that calculated from the fitted function. The width of the residual distribution between the measured and calculated correction is less than 0.1%, which indicates that we understand the correction to at least that level.

V. CDC PERFORMANCE

A. Drift Distance Resolution

The intrinsic drift distance resolution of the chamber (i.e. local to a given drift cell) is determined primarily by the diffusion coefficients of the gas, the ratio of sampling speed to electron drift velocity in the gas, the drift cell design, preamplifier and AMU noise, and the algorithm used to extract the time information from the waveform. Since hits on adjacent wires in a cell are in nearly identical environments, many of the uncertainties which affect the measurement of the absolute position of the hits cancel out if differences of fit residuals of adjacent hits are taken.

The local resolution derived from gaussian fits to the distributions of these differences of residuals is plotted as a function of drift distance in fig. 7. Since only hits on tracks are used in this calculation, and since the fitter can drop hits in the tails of the residual distributions, the results shown here

are for the cores of the distributions. Typically, about 5% of the actual hits lie outside of 4σ of the core. In the region of linear field the resolution follows the curve expected from diffusion (68 μm at 1 cm and varying as $\sqrt{d}$). The mean resolution for hits in this region, and lying on near-radial track segments, is 82 μm.

The global hit residual resolution, and even more importantly, the resolution on the measured track parameters, depend on a knowledge of various systematic effects, such as: the time-to-distance relationship (its variation layer-to-layer as well as with electric field), wire positions, time offsets, and gravitational sag. The alignment of the chamber wires is performed using measured tracks. Selected tracks from hadronic decays of the Z^0 provide information on the deviation of the positions and orientations of individual cells from their nominal values, which leads to a set of a cell-to-cell alignment constants. After this local alignment of the cells is done, we use muon tracks from the decay $Z^0 \rightarrow \mu^+\mu^-$ (di-muon event) to determine the gross rotation of superlayers, by exploiting the fact that the two tracks in such an event should be back-to-back and each have the same momentum as the beam. Figure 7 also shows the global resolution after alignment and corrections. The mean global track resolution for hits in the region of linear drift, and lying on near-radial tracks, is measured to be 92 μm. The difference between the global and local resolution reflects an uncertainty of 30 to 40 μm in alignment and other calibrations, assuming that these effects add in quadrature. Note the degradation of the resolution in the regions near the sense and field wires. This is due mainly to

the increased drift velocity and non-uniformity of the drift field in these regions.

B. Resolving of Close Hits

The ability to resolve two close hits depends on details of the waveform analysis as well as the intrinsic resolution of the chamber electronics. (See fig. 3 for an example of a two-hit waveform.) Our algorithm assigns a second hit when it senses a sufficiently large deviation on the falling edge of the pulse. Because the actual waveform exhibits significant irregularities, the algorithm must be tuned to be reasonably efficient for second hits, while not generating too many second hits where none exist. Figure 8 illustrates the two-hit resolution for the current state of our algorithm. An efficiency of 50% is achieved by a separation of 1 mm, which corresponds to about 15 AMU channels or 120 ns. Approximately 3% of the hits on tracks in Z^0 decays to hadrons are too close to be resolved.

C. dE/dx Resolution

Although the CDC is not designed for optimal energy-loss measurement, we obtain a dE/dx resolution of 6.4% for electrons in wide-angle-Bhabha events, after correcting for geometric effects, diffusion, transport loss, and gain variations. This capability will be useful in some of our analyses.

D. Momentum Resolution

We have calculated the momentum resolution expected for a perfectly efficient chamber with the same material and wire geometry as ours, and with a uniform drift distance resolution of 100 μm. This value was chosen to characterize the average resolution over the entire drift distance of the cell. The result can be parametrized as $(dp_t/p_t^2)^2 = 0.0031^2 + (0.0086/p_t)^2$, where p_t is the track momentum perpendicular to the beam axis. The first term represents the effects of multiple scattering, and the second, those of measurement error.

In the actual chamber, numerous effects, such as hit inefficiencies, misalignments, and tails on drift distance resolutions, conspire to degrade the resolution obtained for real tracks. The resolution at high momentum can be measured using the mono-energetic tracks in the decay $Z^0 \rightarrow \mu^+\mu^-$. Figure 9 shows the distribution of Q/p for such muon tracks. At low momentum, there is no such simple calibration event. However, cosmic rays passing through the CDC may be used for this purpose, by considering the upper and lower halves of each track as two separate tracks; comparing the two measured momenta yields an estimate of the resolution. Using these techniques, we measure the momentum resolution function for the CDC to be $(dp_t/p_t^2)^2 = 0.0050^2 + (0.010/p_t)^2$.

Figure 10 shows a plot of the kaon mass spectrum; its width is consistent with the angular and momentum resolution of the CDC.
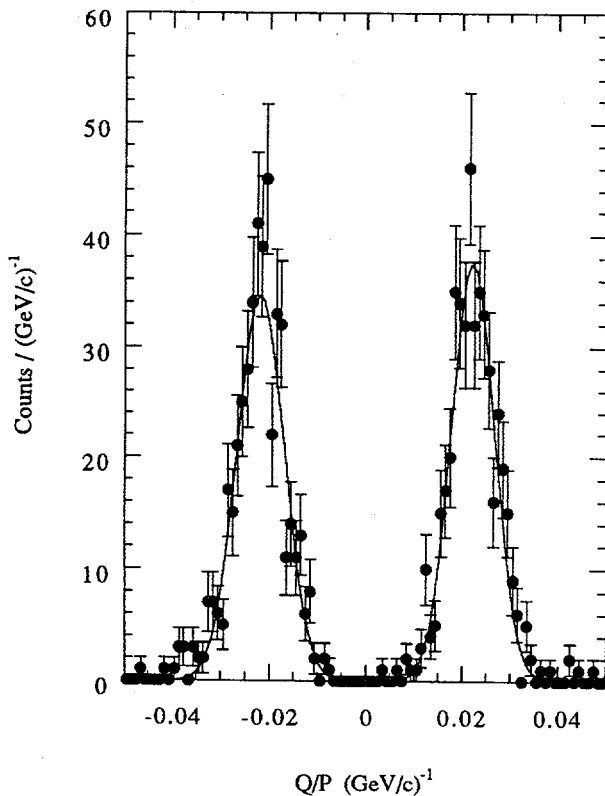

Fig. 9. Distribution of charge over momentum for tracks from $Z^0 \rightarrow \mu^+\mu^-$ decays. The data are fit with one gaussian for each peak.
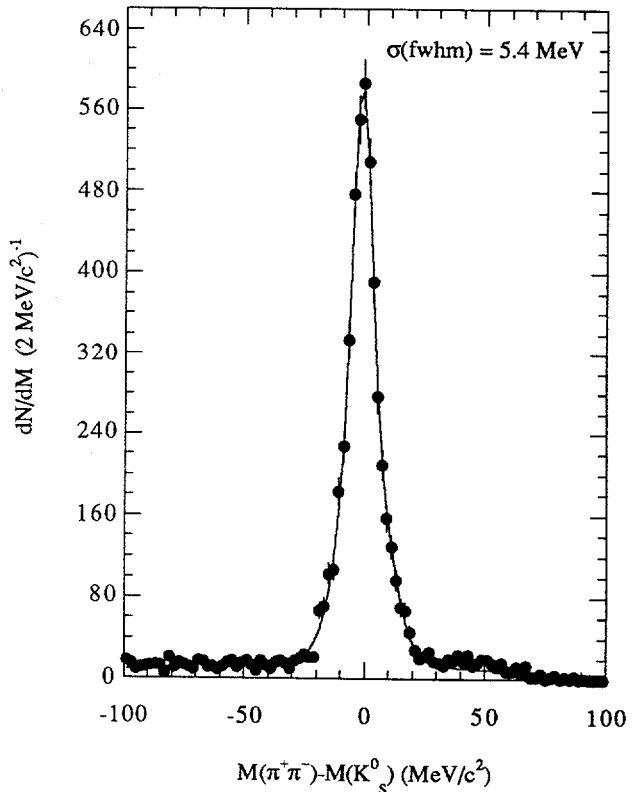

Fig. 10. Kaon mass as measured with tracks with only CDC hits. The curve is a fit using two gaussians and a quadratic background.
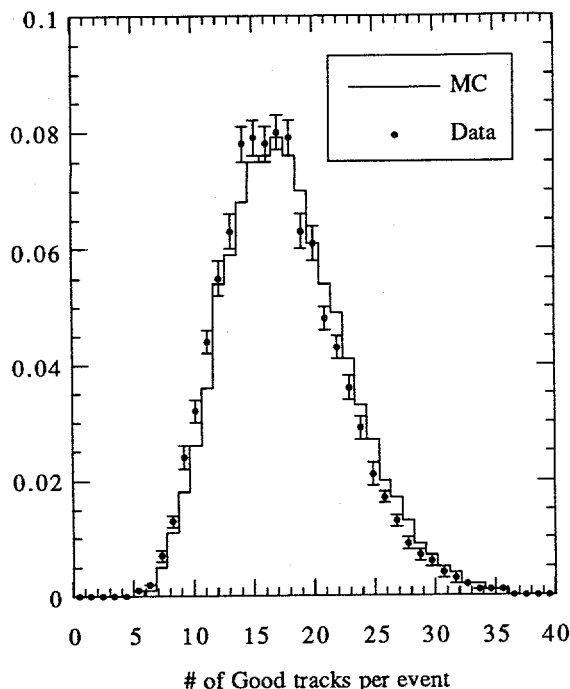
6

Fig. 11. The distribution of the number of tracks reconstructed in the CDC in hadronic Z^0 events for both data and Monte Carlo.

Fig. 12. The efficiency for linking a good CDC track to the vertex detector as a function of momentum.

VI. OVERALL TRACKING SYSTEM PERFORMANCE

The performance of the SLD tracking system is perhaps best characterized by the extent to which it can be used to tag decays of Z^0s into heavy quarks through identification of secondary vertices. In addition to the CDC, this system includes the SLD Vertex Detector[5] (VXD). To exploit the vertexing capability of this system, tracks must be efficiently found in the CDC and linked to pixel clusters in the VXD, then extrapolated to the SLC interaction point. The VXD consists of two effective layers of charge-coupled devices (CCDs) with 22 μm x 22 μm pixels, at radii of 3 and 4 cm, respectively. The beam spot at the SLC is small (2.4 μm x 0.8 μm x 750 μm) and its position is tracked to within 7 μm.

The overall track-reconstruction efficiency is measured in the Monte-Carlo simulation (MC) to be 96%. In fig. 11, we show the distribution of charged-track multiplicity for data, and for events generated in the MC, with tight quality cuts on the tracks counted. A discrepancy of about 0.5 tracks per event can be seen. The disagreement between data and MC turns out to be significant for studies which depend on tagging of heavy flavor through detection of secondary vertices. This is because such analyses are performed by counting, for example, the number of tracks with large impact parameter in an event. If the track multiplicity is different in data and MC, the efficiencies and purities estimated from the MC will be subject to systematic uncertainties.

Figure 12 shows the efficiency for linking the tracks fit in the CDC with hits in the VXD, after tight quality cuts are applied to the CDC tracks. The measured efficiency is about 96% above 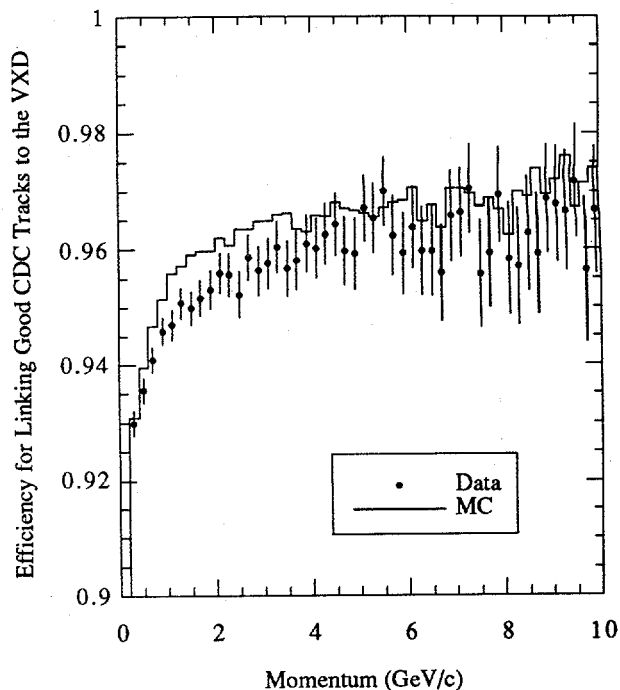a momentum of 4 GeV/c, and falls to 93% at the lowest momentum, as multiple scattering becomes more important. The figure also shows the efficiency calculated from events generated in the MC. Again, the discrepancy feeds into our estimates of systematic uncertainty in some of our analyses.

The two-prong miss distance is the distance of closest approach between the extrapolations of the two tracks in di-muon events at their point of closest approach; dividing this number by $\sqrt{2}$ gives a measurement of the resolution in the track position at the interaction point. Fits to CDC data alone yield $\sigma_{r\phi}$= 155 μm and σ_z= 1.9 mm for the resolutions. The poorer resolution of the z component is due to the ±41 mrad stereo angle which is used to measure it. Adding the linked VXD hits to the fits dramatically improves these resolutions, yielding $\sigma_{r\phi}$= 10 μm and σ_z= 36 μm. Without the CDC, the relatively small separation of the VXD layers would limit the resolution to 48 μm in both views, even if it were somehow possible to actually do tracking in the 2 layers of the VXD.

The impact parameter of a track is its distance of closest approach to the interaction point, signed by the hemisphere of the jet to which it belongs. Its quality is determined by how well one can measure the position of the interaction point and how well one can extrapolate the tracks. In spite of the already-mentioned discrepancy between data and MC, understanding of CDC systematics is now at a level where we can compare the measured and simulated impact parameter distributions for hadronic Z^0 events and get excellent agreement, without the need for additional ad hoc smearing in the MC, as can be seen in fig. 13. This allows for the extraction of physics results with minimal systematic errors from this source.
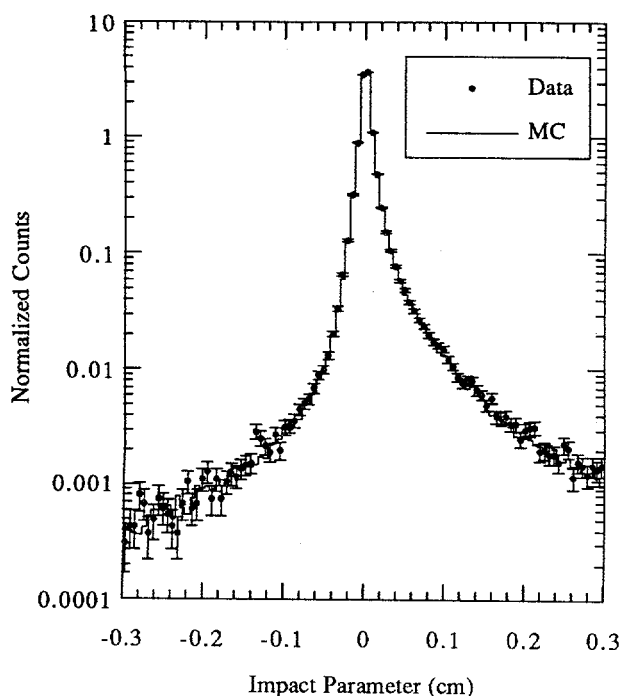
7

Fig. 13. The impact parameter distribution of tracks in Z^0 decays for data and Monte Carlo. The two distributions are in excellent agreement over 4 orders of magnitude, without the need for ad-hoc smearing of the track parameters.

VII. CONCLUSIONS

The Central Drift Chamber of the SLD detector has proved to be robust and reliable, and is now performing at a level approaching its design specifications. At the present stage of data-taking, the errors in our physics results are still typically dominated by statistics, but as the statistical power of our measurements increase, we will need to improve the our understanding of the tracking efficiency. The larger data sample will help us to do this.

In addition, the installation, in late 1995, of an improved VXD, with three layers and increased angular coverage, will augment the capabilities of the tracking system. It should also allow us to use the CDC more effectively, and help us to improve our understanding of its performance, by providing independent tracking.

ACKNOWLEDGMENTS

REFERENCES

(a) Presently at LAPP, F-74941 Annecy-le-Vieux, France
(b) Presently at Nagoya University, Nagoya 464, Japan
(c) Presently at Hiroshima University, Higashi-Hiroshima 724, Japan
(d) Presently at University of California at Santa Cruz, Santa Cruz, CA 95064

[1] J.P. Venuti and G.B. Chadwick, "Radiation Aging Studies of CO_2 Hydrocarbon Mixtures for the SLD Drift Chamber," *IEEE Trans. on Nucl. Sci.,* vol. 36, pp. 595-599, February 1989.

[2] G.M. Haller *et al.,* "Physical Packaging and Organization of the Drift Chamber Electronics System for the Stanford Large Detector," *IEEE Trans. on Nucl. Sci.,* vol. 38, pp. 357-362, February 1991; G.M. Haller *et al.,* "The Front-End Analog and Digital Signal Processing Electronics for the Drift Chambers of the Stanford Large Detector," *ibid.,* pp. 363-369; A. Honma *et al.,* "Performance of the Front-End Signal Processing Electronics for the Drift Chambers of the Stanford Large Detector," *ibid.,* pp. 370-375.

[3] J. T. Walker *et al.,* "Microstore - the Stanford Analog Memory Unit," *IEEE Trans. on Nucl. Sci.,* vol. 32, pp. 616-621, February 1985; D.R. Freytag and J.T. Walker, "Performance Report for SLAC/STANFORD Microstore Analog Memory Unit," *ibid.,* pp. 622-625.

[4] S. MacKenzie *et al.,* "The Digital Correction Unit: A Data Correction/Compaction Chip," *IEEE Trans. on Nucl. Sci.,* vol. 34, pp. 250-252, February 1987.

[5] C.J. Damerell *et al.,* "Design and Performance of the SLD Vertex Detector, a 120 MPixel Tracking System," *Proceedings of the 26th International Conference on High Energy Physics,* Dallas, TX, August 1993, pp. 1862-1866.